Materials Science-Poland, 33(1), 2015, pp. 47-55
http://www.materialsscience.pwr.wroc.pl/
DOI: 10.1515/msp-2015-0008

DE GRUYTER OPEN

Synthesis of SiO_2 nanopowders containing quartz and cristobalite phases from silica sands

MUNASIR[1,2*], TRIWIKANTORO[1], MOCHAMAD ZAINURI[1], DARMINTO[1]

[1]Department of Physics, Faculty of Mathematics and Sciences, Institut Teknologi Sepuluh Nopember (ITS), Kampus ITS Sukolilo, Surabaya 60111, Indonesia

[2]Department of Physics, Universitas Negeri Surabaya (UNESA), Kampus UNESA Ketintang, Surabaya 60231, Indonesia

In this study, extraction and synthesis of SiO_2 nanoparticles from silica sands have been conducted by means of two different methods, i.e. dry method (method 1) and hydrothermal process (method 2). The basic difference between the two methods is in the extraction step. The two methods were compared in terms of being more efficient, economical, and superior in obtaining SiO_2 nanoparticles. The SiO_2 nanoparticles were characterized in terms of phase purity, crystallinity, Si–O functional bonding as well as particles size and morphology. The most interesting fact in this study was the formation of both quartz and cristobalite phases within all prepared SiO_2 nanoparticles.

Keywords: *silica sand; SiO_2 nanoparticles; quartz and cristobalite phases*

1. Introduction

Silica (SiO_2) naturally exists in three main phases, i.e. quartz, tridymite, and cristobalite, and five minor phases, i.e. keatite, coesite, melanophlogite, fibrous and faujasite [1]. Silica itself has been used as a raw material in many industries of glasses, mirrors, mosaic ceramics, ferro silicon, silicon carbide for abrasives and sand blasting. It is also widely employed as a supporting material in industries of cast steel, oil and mining, and refractory brick. Silica with calcium additive has grown to be a new nano-composite as a bioactive material for bone tissue replacement [2]. Besides, other potential applications of silica nanoparticles are in areas of pigment production, pharmaceutical and catalyst industries [3]. Silica can also be applied for reinforcing polymer composites in coatings for corrosion protection and plastic bags [4], composite polymer gel electrolytes [5, 6], thermoplastic polymers [7], and volatile flavor compounds [8].

Chemical processes, such as extractions, purifications, and syntheses of SiO_2 nanoparticles based on natural materials have been widely conducted. For instance, amorphous silica nanoparticles with purity of more than 95 % have been prepared by means of chemical methods (sol gel and hydrothermal) using organic materials, like baggase ash [4] and rice hush ash [3, 9]. Meanwhile, inorganic materials, like silica sands have been employed to produce SiO_2 nanoparticles via high energy milling [10]. Diorite sand with Na_2CaO_3 addition was sintered at temperature of 1030 °C [11]. Waste colored glass has also been used for obtaining SiO_2 nanoparticles by means of extraction process using alkali compounds KOH and NaOH at sintering temperatures of 360 and 500 °C to form sodium silicate (Na_2SiO_3) [12, 13]. Other researchers have prepared SiO_2 nanoparticles from commercial raw materials [14–17]. However, a synthesis approach to produce SiO_2 nanoparticles from inorganic materials or silica sands has not been reported so far.

The SiO_2 nanoparticles are commonly synthesized by means of various approaches, for instance, precipitation [18, 19], aggregation [20], emulsion [15], and sol-gel [21]. In the present

*E-mail: munasir09@mhs.physics.its.ac.id

study, we introduce two different methods of synthesizing SiO_2 nanoparticles from a local natural resource of silica sands. In general, with the particle size of around ∼200 mesh, silica sand in nature has various purities, depending on the impurities. Oxide minerals containing Fe, K, Mg, and Ca as well as organic materials from animals or plants are the impurities in silica sands, influencing further their color. Silica sands formed by rock weathering contains quartz minerals, like granite, granodiorite, diorite, and quartzite. The sedimentary rock, formed due to weathering and erosion, experiences transportation, and natural watery (e.g. by rain or river water) resulting in finer and cleaner grains of silica sand, which is finally precipitated on the beach [22]. The methods employed in this study include dry method (method 1) and hydrothermal method (method 2).

2. Experimental method

The raw materials used in this study were silica sands from Bancar (Tuban, Indonesia), NaOH (99 %), HCl (37 %) and DI water.The synthesis steps for method 1 were: (i) purification of SiO_2 from impurities using alkali media (dry process) by mixing silica sand powders and NaOH with compositions of x wt.% SiO_2 and (100−x) wt.% NaOH followed by heating at a temperature of 500 °C to form solid sodium silicate ($Na_2O{\cdot}xSiO_2$); (ii) titrating sodium silicate solution with HCl (1 M) until reaching normal pH and producing silicite ($Si(OH)_4$) in a gel form, (iii) cleaning with DI water to release NaCl from silica precipitate, and (iv) drying the precipitate at a temperature of 80 °C for 24 hours.

In the method 2, formation of solid sodium silicate via hydrothermal process was required. The synthesis steps for method 2 were: (i) silica sand powder was mixed with 5 M, 6 M, and 7 M NaOH solution and then stirred thoroughly at a temperature of 90 °C for 2 hours to obtain $Na_2{\cdot}xSiO_3$ used as a precursor, (ii) formation step to produce silicite, titrating sodium silicate solution with HCl (1 M) until reaching normal pH (∼7), (iii) the next step was the same as in the method 1.

The as-prepared SiO_2 powders were then characterized by means of X-ray diffractometry (XRD) to investigate the phase formation and crystal structure [23], X-ray fluouresence (XRF) to evaluate the elemental composition [24], fast-Fourrier transform infra-red spectrometry (FT-IR) to study the silica functional groups [25], scanning and transmission electron microscopy (SEM and TEM) to demonstrate the morphological and microstructural properties [7, 26], and Brunauer-Emmett-Teller (BET) to determine the surface area [27].

3. Results and discussion

3.1. Characterizations of silica sand

The result of XRF analysis of silica sand samples from two different sampling locations in Bancar is shown in Table 1. It indicates that the predominant elements are Si, Ca, and K with the percentage contributions of 59 %, 34.9 %, and 2.69 %, respectively; and their corresponding oxides, which are SiO_2, $CaCO_3$, and K_2O of 76.80 %, 20.50 %, and 1.45 %, respectively.

Fig. 1 shows the XRD patterns of natural silica sands (#1), silica sands after being washed with HCl (#2), and SiO_2 product from natural silica sands after completing the hydrothermal process (#3). An automatic phase identification was conducted by High Score Plus software and it revealed the presence of quartz (PDF2 No. 01-087-2096), microcline (PDF2 No. 01-071-1540), and calcite (PDF2 No. 01-083-1762) for the XRD data in Fig. 1 (#1) and (#2), and only quartz for Fig. 1 (#3). Further semi-quantitative phase analysis carried out using RIR method [28] showed that the content of quartz increased when the hydrothermal process was completed. We obtained 66.7 %, 77.0 % and 100.0 % of quartz for the XRD data shown in Fig. 1 (#1), (#2), and (#3), respectively. After HCl immersion, the amount of microcline remained almost unchanged, whereas the amount of calcite within the sample decreased significantly (Table 2). The completion of hydrothermal process led to the complete removal of calcite and microcline, and consequently, only quartz remained. Finally, we have produced crystalline SiO_2 from

Table 1. XRF data analysis of the silica sands from Bancar.

Raw material	Atomic wight (%)								
	Si	Ca	K	Fe	Ni	Ti	Cu	Ba	Others
(#1)	59.00	34.90	2.69	1.34	0.00	0.00	1.00	0.20	<0.01
(#2)	82.00	15.20	1.02	0.14	0.00	0.00	0.01	0.00	<0.01
(#3)	97.16	0.80	1.10	0.38	0.04	0.36	0.08	0.00	<0.01

Note: (#1) natural silica sands (NSS) form Bancar-Indonesia; (#2) NSS after HCl treatment; and (#3) SiO_2 obtained from NSS via hydrothermal process.

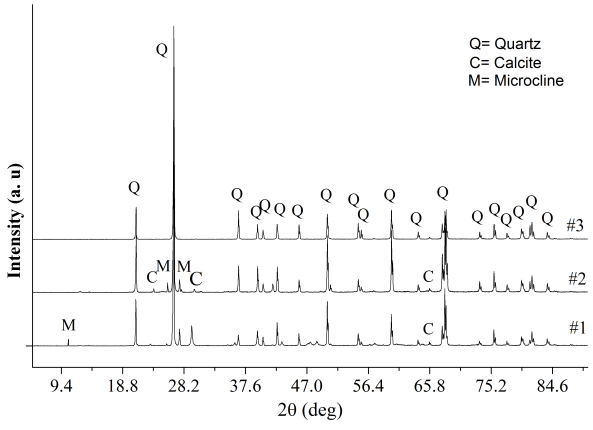

Fig. 1. XRD patterns of (#1) natural silica sand, (#2) natural silica sand after HCl treatment, and (#3) silica obtained from natural silica sand via hydrothermal process.

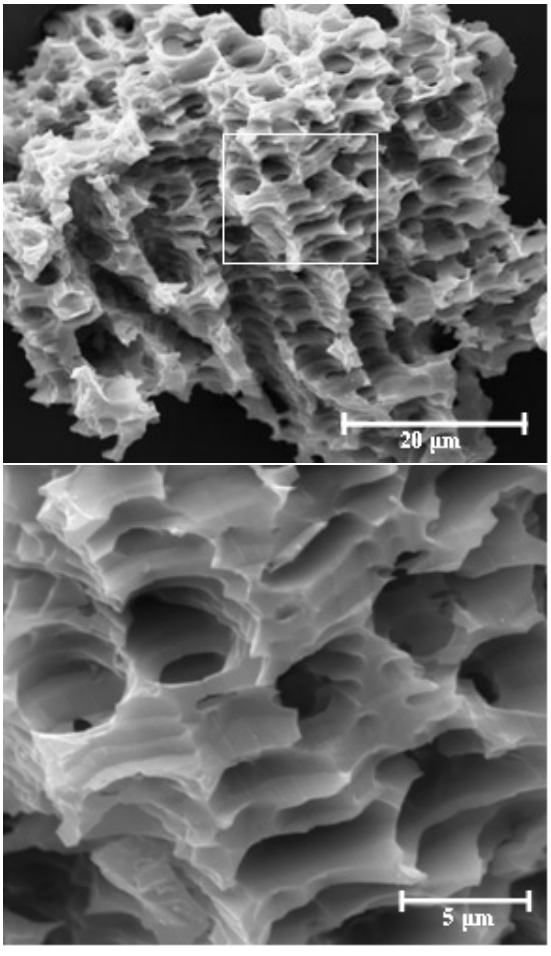

Fig. 2. Micrograph and its zooming in image of pure quartz from natural silica sands obtained via hydrothermal process (#3 sample).

silica sands by means of hydrothermal route. In Fig. 2, we can see the product after the first-step process (i): the crystalline SiO_2 is well shaped with regular pores. It shows the ability of hydrothermal route to produce quartz of very high purity from natural silica sands. The size of the pores and the crystallites is of the order of micrometer. The SEM micrograph strongly supports the X-ray diffraction data in Fig. 1.

3.2. Characterization of SiO_2 product

The XRD patterns of SiO_2 produced by method 1 and method 2 are given in Fig. 3a and 3b, respectively. In method 1, the samples with different silica sand to sodium hydroxide ratios (in wt.%) were used: (i) 10:90 for NS(1), (ii) 15:85 for NS(2), and (iii) 12.5:87.5 for NS(3). In method 2, the samples had different sodium hydroxide solution molarities: (iv) 5M NaOH for NS(4), (v) 6M NaOH for NS(5) and (vi) 7M NaOH for NS(6). A visual analysis clearly shows that the XRD patterns obtained for the samples produced by either method

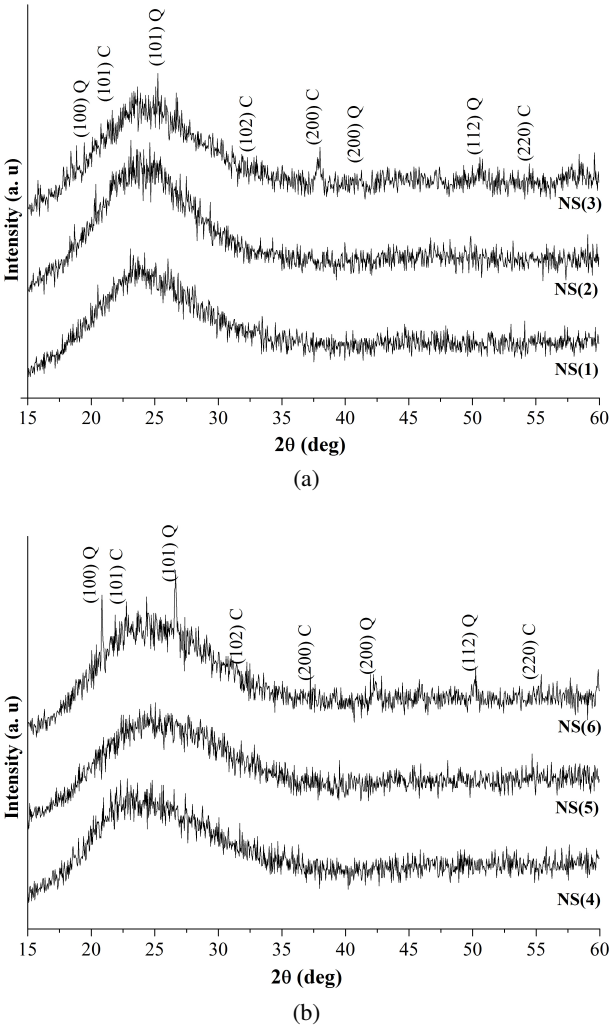

Fig. 3. XRD patterns of the SiO_2 nanoparticle sampels obtained by (a) method-1: NS(1), NS(2), NS(3) and (b) method-2: NS(4), NS(5), NS(6).

1 or method 2 consist of amorphous phase and a small amount of crystalline phase.

The XRD data of the amorphous silica show the much broader diffused peak. From Fig. 3a, it is clearly seen that the increasing content of NaOH causes a peak shift to the lower 2θ, which is similar to that in Fig. 3b. This result is also in a good agreement with the previous reports [11, 12]. Furthermore, after executing automatic search-match crystalline phase analyses, we made an important discovery that there exists not only quartz (PDF2 No. 01-087-2096) but also cristobalite (PDF2 No. 01-082-1408) in the SiO_2 product. It is, however, rather surprising that the cristobalite has also grown in the prepared samples. In addition, to accomplish the XRD data analysis, the hkl indices of each phase are also given explicitly in Fig. 2, which is further confirmed by TEM image (below). Another analysis to quantify the degree of crystallinity was executed by applying quantitative analysis using external standard method. The analysis revealed that the amounts of crystalline phase of NS(3) and NS(6) were 19.84 % and 17.99 %, respectively. Meanwhile, the estimated crystallite size was calculated by the well-known Scherrer formula [28–30], that yielded 81 nm for NS(3) and 67 nm for NS(6).

Continuing FT-IR evaluations, the spectra and the spectral data of produced silica powders are presented in Fig. 4 and Table 4. The IR band at 3437 cm^{-1} is due to the stretching vibration of H_2O molecules. Correspondingly, the IR band at 1632 cm^{-1} is assigned to –OH bending vibrations of H_2O molecules. The shoulder at 3246 cm^{-1} could be assigned to the stretching vibrations of Si–OH groups in the structure of amorphous SiO_2 [31]. The presence of the Si–OH group is an evidence of forming bonded water. The very strong and predominant absorbance peaks at 1082.8 to 1099.1 cm^{-1} range are usually assigned to the TO and LO modes of the Si–O–Si asymmetric stretching vibrations. The IR band at 956 cm^{-1} can be assigned to silanol groups. In the case of alkali silicate glasses, this band is assigned to Si–O– stretching vibrations. The IR band at 800 cm^{-1} can be assigned to Si–O–Si symmetric stretching vibrations, whereas the IR band at 474 cm^{-1} is due to O–Si–O bending vibrations. Previous study revealed that Si–O group lies in a wave number range of 465 to 475 cm^{-1}, Si–OH group in 800 to 870 cm^{-1}, siloxane Si–O–Si group in 1115 to 1050 cm^{-1}, water molecule O–H group in 1625 cm^{-1} and O–H group in 3000 to 4000 cm^{-1} [16, 17, 31].

Table 5 presents the elemental constituents of produced silica [(NS(1), NS(2), NS(3), (NS(4), NS(5), and NS(6)]. The samples of NS(1), NS(2) and NS(3) were prepared by the method 1, titrating $Na_2{\cdot}xSiO_2$ solution with HCl at neutral pH (∼7).

Table 2. Semi-quantitative phase analysis results of XRD data from Fig. 1.

Samples	Ref. Code	Phase	Chemical formula	Quantification (based on RIR method)
(#1)	01-087-2096	Quartz	SiO_2	66.7 %
	01-071-1540	Microline	$K(Al,Fe)Si_3O_8$	13.1 %
	01-083-1762	Calcite	$CaCO_3$	20.2 %
(#2)	01-087-2096	Quartz	SiO_2	77.0 %
	01-071-1540	Microline	$K(Al,Fe)Si_3O_8$	13.0 %
	01-083-1762	Calcite	$CaCO_3$	10.0 %
(#3)	01-087-2096	Quartz	SiO_2	100.0 %

Table 3. Semi-quantitative phase analysis of XRD patterns of the SiO_2 samples for NS(4) and NS(6) applying high score plus software.

h k l	2θ (°)	d-spacing (Å)	Matched phase		Characterized by	
			Quartz (01-087-2096)	Cristobalite (01-082-1408)	XRD	TEM
(101)	26.6733	3.34213	√		√	√
(102)	31.8600	2.80889		√	√	√
(200)	36.8285	2.44057		√	√	√
(200)	42.3400	2.13475	√		√	√
(220)	55.4600	1.65684		√	√	√

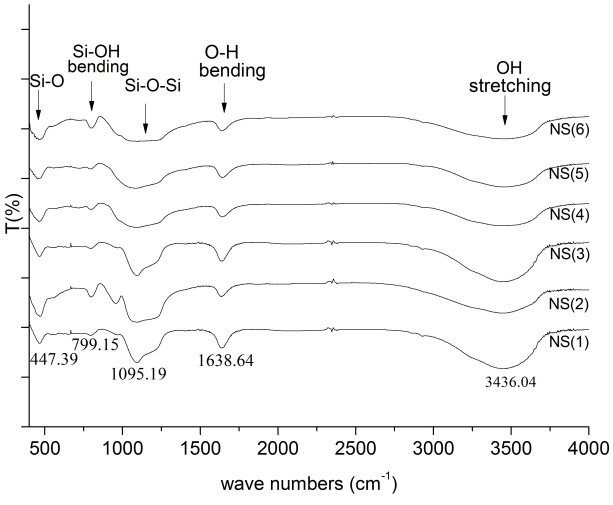

Fig. 4. FT-IR spectra of the SiO_2 nanoparticles, method-1: NS(1), NS(2), NS(3) and method-2: NS(4), NS(5), and NS(6).

Silica gel was obtained from NS(1) with silica content of 72.9 % followed by reduction of CaO, K_2O and Fe_2O_3, which were not completely removed. The NS(2) sample was synthesized by the same way as that of NS(1), but controlling pH between 1 and 2. The elemental content for NS(2) can be found in Table 4. The SiO_2 content in NS(2) sample is very high, i.e. 94.8 %. The NS(3) sample was produced by soaking the sand powders with 2M HCl for 10 hours to dissolve contaminants. The loss of impurities after the soaking is indicated by the mass reduction from 7 g to 6.2 g. Using this method, we obtained SiO_2 with the purity as high as 98.9 % and impurities content of 0.42 % CaO and 0.237 % Fe_2O_3.

The samples of NS(4), NS(5), and NS(6) were prepared by the method 2, NS(4) was synthesized at pH = 1 (stopping titration) resulting in high purity silica (97.10 %); NS (5) was synthesized at pH = 4 (stopping titration) resulting in high purity silica (96.10 %); and NS(6) was synthesized at pH = 7 (stopping titration) resulting in high purity silica (98.30 %), with reduction impurities of

Table 4. Assignment of infra red (IR) spectral data of silica.

Frequency (cm^{-1})						Position assignment	Frequency value (cm^{-1}) (from literature)	Ref.
Method 1			Method 2					
NS(1)	NS(2)	NS(3)	NS(4)	NS(5)	NS(6)			
477.4	470.9	467.3	466.0	465.2	463.1	Group Si–O (siloxy)	465 – 475	[17, 31]
799.2	799.1	795.9	797.1	798.3	799.1	Group Si–OH (silanol)	800 – 870	[16, 17]
1095.2	1095.4	1082.8	1099.1	1096.2	1095.5	Group Si–O–Si (siloxane)	1115 – 1050	[16, 31]
1638.6	1638.8	1639.1	1639.8	1639.3	1639.0	Group O–H (water molecule)	1625	[17]
3436.1	3437.3	3469.5	3467.9	3466.1	3467.6	Group –OH (silanol)	3000 – 4000	[16, 17]

Table 5. XRF data analysis of the SiO_2 samples obtained by method 1 (NS(1), NS(2) and NS(3)) and method 2 (NS(4), NS(5) and NS(6)).

Samples of silica product		Atomic weight (%)					Oxide weight (%)				
		Si	Ca	K	Fe	Others	SiO_2	CaO	K_2O	Fe_2O_3	Others
Method 1	NS (1)	71.86	4.42	15.21	1.12	<0.10%	72.90	5.74	16.60	2.22	<0.10%
	NS (2)	92.18	0.23	0.08	2.22	<0.10%	94.80	0.65	0.20	2.11	<0.10%
	NS (3)	96.50	0.38	0.23	0.32	<0.10%	98.90	0.42	0.49	0.23	<0.10%
Method 2	NS (4)	95.00	1.00	0.16	2.68	<0.10%	97.10	0.63	0.12	1.52	<0.10%
	NS (5)	95.60	1.10	0.25	1.60	<0.10%	96.10	0.47	0.00	2.77	<0.10%
	NS (6)	95.70	0.98	0.10	1.44	<0.01%	98.30	0.55	0.06	0.65	<0.10%

Ca, K, and Fe elements or CaO, K_2O and Fe_2O_3 oxides.

The microstructures of the NS(3) and NS(6) samples are given in Fig. 5. At 60,000 magnification, we can clearly see some agglomerated SiO_2 particles with sphere-like morphology, having particle size of around 72 nm. Further analysis by means of "*image-j software*" and BET measurement gave estimated surface area, diameter, and particle size (Table 6). Taking an assumption that SiO_2 nanoparticles are spherical, nonporous, and uniform in shape, the theoretical surface area of a particle can be calculated by the following equation [26, 31]:

$$S = (6/\rho D) \tag{1}$$

where ρ represents the particle density ($\rho = 2.0 \times 10^6$ g/m^3 for silica) and D corresponds to particle diameter. The calculated S values in comparison to the experimental value from BET measurement are listed in Table 6.

The morphology of SiO_2 nanoparticles for NS(3) and NS(6) are given in Fig. 6. The synthesis methods influenced the particle size and surface area of SiO_2 nanoparticles (Table 4). TEM image shows that the particles are of nanometer size. The uniformly spherical particles tend to form agglomerated species. The diffuse ring pattern indicates the presence of amorphous phase in addition to the main phase (Fig. 6a) [9]. Meanwhile, Fig. 6b indicates the formation of crystalline state within the SiO_2 nanoparticle. The XRD data related to NS(6) inform that the crystalline phases within the sample are quartz and cristobalite. Recalling the full pattern analysis on the XRD data at this point, an explicit comparison can be done to confirm validity of the analysis. From Table 2 and Fig. 6 one can see that besides amorphous silica, quartz and cristobalite actually coexist in the sample.

4. Conclusions

The SiO_2 nanoparticles have successfully been synthesized from natural silica sands by means of dry and hydrothermal methods. From the viewpoint of process duration, lowering temperature and cost,

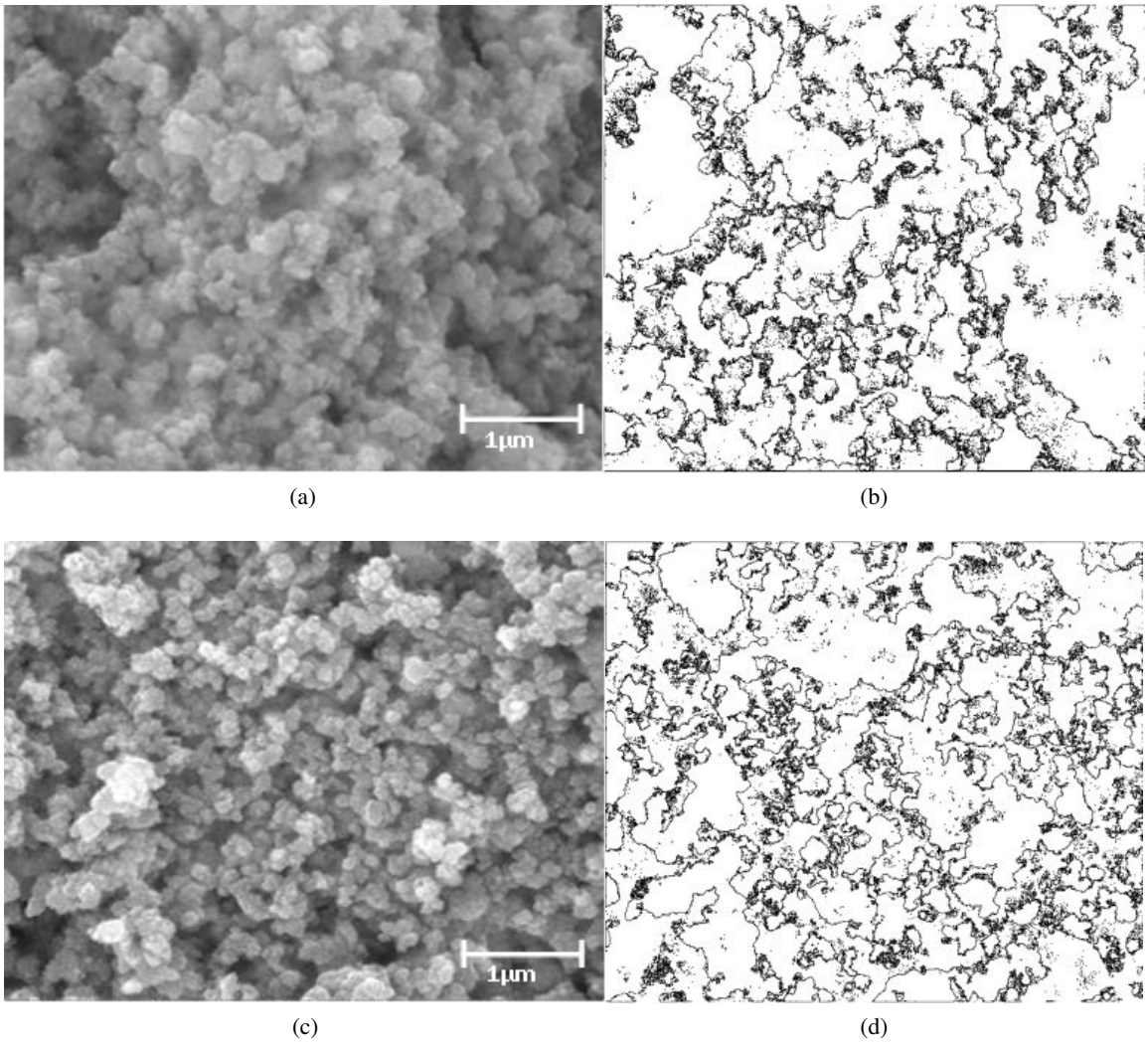

Fig. 5. SEM and outline images of the SiO_2 for: (a) and (b) – NS(3); and (c) and (d) – NS(6) samples.

Table 6. Surface area and particle size of SiO_2 product.

Samples of silica product	Samples	Average particle size, D (nm)[a]	Surface area, S(m^2/g)[c]	Surface area, S(m^2/g)[b]
Method 1	NS(1)	49.2	60.1	43.0
	NS(2)	48.9	61.3	45.2
	NS(3)	50.0	60.0	46.7
Method 2	NS(4)	32.1	93.4	56.6
	NS(5)	30.3	99.2	59.0
	NS(6)	29.1	103.1	63.3

[a]analysis with image-j software. [b]Surface area calculated based on spherical model (theoretical: equation 1). [c]BET of surface area (m^2/g).

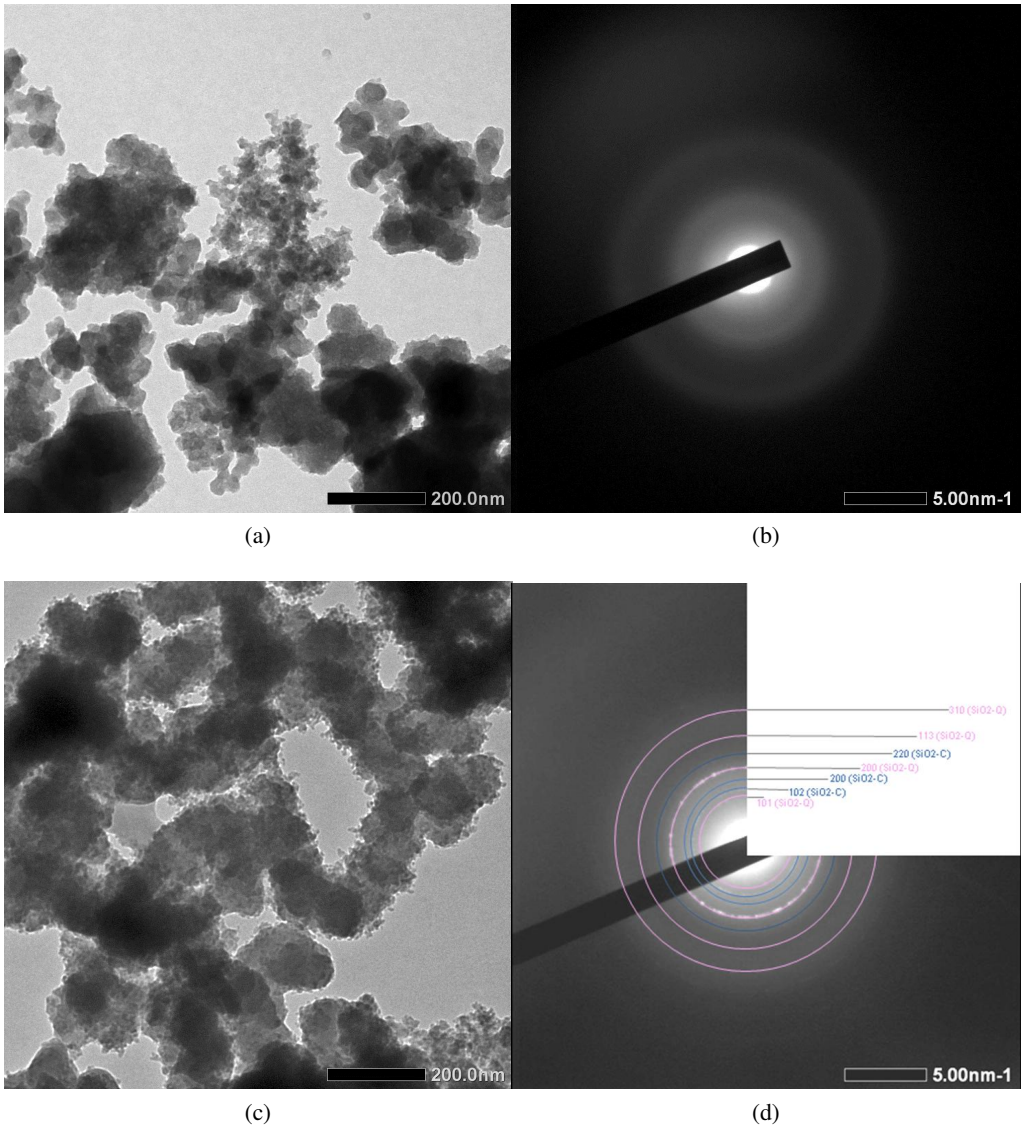

Fig. 6. TEM with electron diffraction images of SiO_2 nanoparticles: (a) and (b) – NS(3); and (c) and (d) – NS(6).

the latter method is strongly recommended as compared to the former one. Using this method we obtained high purity SiO_2 (more than 98 %) composed of spherically shaped particles with the size of around 30 nm, containing quartz and cristobalite phases. The presence of the silanol (Si–O), siloxane (Si–O–Si) as well as hydroxyl groups on the surface of the tested samples was revealed.

Acknowledgements

This work was partly supported by Institut Teknologi Sepuluh Nopember of Surabaya (ITS). One of the authors (M) is grateful for the supports from Universitas Negeri Surabaya (UNESA) and the Ministry of Education and Culture of Indonesian Republic to provide BPPS scholarship for doctoral program.

References

[1] HONG Z., LIU A., CHEN L., CHEN X., JING X., *J. Non-Cryst. Solids*, 355 (2009), 368.

[2] JANG H.D., CHANG H.K., YOON H.S., CHO K., PARK J.H., OH S.Y., *Colloid. Surface. A*, 313 – 314 (2008), 121.

[3] KALAPATHY U., PROCTOR A., SHULTZ J., *Bioresource Technol.*, 85 (2002), 285.

[4] AFFANDI S., SETYAWAN H., WINARDI S., PURWANTO A., BALGIS R., *Adv. Powder Technol.*, 20 (2009), 468.

[5] WALKOWIAK M., ZALEWSKA A., JESIONOWSKI T., POKORA M., *J. Power Sources*, 173 (2007), 721.
[6] OSIŃSKA M., WALKOWIAK M., ZALEWSKA A., JESIONOWSKI T., *J. Membrane Sci.*, 326 (2009), 582.
[7] JESIONOWSKI T., BULA K., JANISZEWSKI J., JURGA J., *Compos. Interface.*, 10 (2003), 225.
[8] DZIADAS M., NOWACKA M., JESIONOWSKI T., JELEŃ H.H., *Anal. Chim. Acta*, 699 (2011), 66.
[9] NITTAYA T., NUNTIYA A., *Chiang Mai J. Sci.*, 35 (1) (2008), 206.
[10] AHMAD T., MAMAT O., AHMAD R., *J. Nanoparticles*, 2013 (2013), 1.
[11] TRABELSI W., BENZINA M., BOUAZIZ S., *Phys. Procedia*, 2 (2009), 1461.
[12] MORI H., *J. Ceram. Soc. Jpn.*, 111 (2003), 376.
[13] MUNASIR Z., SULTON A., TRIWIKANTORO T., ZAINURI M., DARMINTO D., *AIP Conf. Proc.*, 1555 (2013), 28.
[14] YU K., GUO Y., DING X., ZHAO J., WANG Z., *Mater. Lett.*, 59 (2005), 4013.
[15] JESIONOWSKI T., *J. Mater. Process. Tech.*, 203 (2008), 121.
[16] WASEEM M., MUSTAFA S., NAEEM A., SHAH K.H., SHAH I., IHSAN-UL-HAQUE., *J. Park. Mater. Soc.*, 3 (1) (2009), 19.
[17] RAHMAN I.A., VEJAYAKUMARAN P., SIPAUT C.S., ISMAIL J., CHEE C.K., *Ceram. Int.*, 34 (2008), 2059.
[18] KRYSZTAFKIEWICZ A., RAGER B., JESIONOWSKI T., *J. Mater. Sci.*, 32 (1997), 1333.
[19] SCHLOMACH J., KIND M., *J. Colloid Interf. Sci.*, 277 (2004), 316.
[20] SCHAER E., RAVETTI R., PLASARI E., *Chem. Eng. Process.*, 40 (2001), 277.
[21] TABATABAEI S., SHUKOHFAR A., AGHABABAZADEH R., MIRHABIBI A., *J. Phys.-Conf. Ser.*, 26 (2006), 371.
[22] HOSOKAWA M., NOGI K., NAITO M., YOKOYAMA T., *Nanoparticle Technology Handbook*, Elsevier Science, Oxford, 2007.
[23] DITTRICH H., BIENIOK A., *Measurement Methods. Structural Properties: X-Ray and Neutron Diffraction*, in Garche J. (Ed.), *Encyclopedia of Electrochemical Power Sources*, Elsevier, Amsterdam, 2009, p. 718.
[24] BECKHOFF B., KANNGIESSER B., LANGHOFF N., WEDELL R., WOLFF H., *Handbook of Practical X-Ray Fluorescence Analysis*, Springer-Verlag, Berlin – Heidelberg, 2006.
[25] KLAPISZEWSKI Ł., ZDARTA J., SZATKOWSKI T., WYSOKOWSKI M., NOWACKA M., SZWARC-RZEPKA K., BARTCZAK P., SIWIŃSKA-STEFAŃSKA K., EHRLICH H., JESIONOWSKI T., *Cent. Eur. J. Chem.*, 12 (2014), 719.
[26] UI S.W., LIM S.J., LEE S.H., CHI S.C., *J. Ceram. Process. Res.*, 10 (4) (2009), 553.
[27] MATSUMOTO A., TSUTSUMI K., SCHUMACHER K., UNGER K. K., *Langmuir*, 18 (2002), 4014.
[28] SNYDER R.L., *Powder Diffr.*, 7 (1992), 186.
[29] WASEDA Y., MATSUBARA E., SHINODA K., *X-Ray Diffraction Crystallography*, Springer-Verlag, Heidelberg – Dordrecht – London – New York, 2011.
[30] SHADE J.O., *X-Ray Characterisation of Nanostructured Material*, S3 Thesis, Department of Chemistry, Technical University of Denmark, 2007.
[31] JAL P.K., SUDARSHAN M., SAHA A., PATEL S., MISHRA B.K., *Colloid. Surface A.*, 240 (2004), 173.

Received 2014-03-19
Accepted 2014-10-12